

^{99m}Tc Hynic-rh-Annexin V scintigraphy for in vivo imaging of apoptosis in patients with head and neck cancer treated with chemoradiotherapy

Frank J. P. Hoebbers · Marina Kartachova ·
Josien de Bois · Michiel W. M. van den Brekel ·
Harm van Tinteren · Marcel van Herk ·
Coen R. N. Rasch · Renato A. Valdés Olmos ·
Marcel Verheij

Received: 22 June 2007 / Accepted: 28 September 2007 / Published online: 10 November 2007
© Springer-Verlag 2007

Abstract

Purpose The purpose of this study was to determine the value of ^{99m}Tc Hynic-rh-Annexin-V-Scintigraphy (TAVS), a non-invasive in vivo technique to demonstrate apoptosis in patients with head and neck squamous cell carcinoma. **Methods** TAVS were performed before and within 48 h after the first course of cisplatin-based chemoradiation.

F. J. P. Hoebbers (✉) · J. de Bois · M. van Herk ·
C. R. N. Rasch · M. Verheij
Department of Radiotherapy,
The Netherlands Cancer Institute/Antoni van Leeuwenhoek Hospital,
Plesmanlaan 121,
1066 CX Amsterdam, The Netherlands
e-mail: f.hoebbers@nki.nl

M. Kartachova · R. A. Valdés Olmos
Department of Nuclear Medicine,
The Netherlands Cancer Institute/Antoni van Leeuwenhoek Hospital,
Plesmanlaan 121,
1066 CX Amsterdam, The Netherlands

M. W. M. van den Brekel
Department of Head and Neck Oncology and Surgery,
The Netherlands Cancer Institute/Antoni van Leeuwenhoek
Hospital and Academic Medical Center,
Plesmanlaan 121,
1066 CX Amsterdam, The Netherlands

H. van Tinteren
Biometrics Department,
The Netherlands Cancer Institute/Antoni van Leeuwenhoek Hospital,
Plesmanlaan 121,
1066 CX Amsterdam, The Netherlands

Radiation dose given to the tumour at the time of post-treatment TAVS was 6–8 Gy. Single-photon emission tomography data were co-registered to planning CT scan. Complete sets of these data were available for 13 patients. The radiation dose at post-treatment TAVS was calculated for several regions of interest (ROI): primary tumour, involved lymph nodes and salivary glands. Annexin uptake was determined in each ROI, and the difference between post-treatment and baseline TAVS represented the absolute Annexin uptake: Delta uptake (ΔU).

Results In 24 of 26 parotid glands, treatment-induced Annexin uptake was observed. Mean ΔU was significantly correlated with the mean radiation dose given to the parotid glands ($r=0.59$, $p=0.002$): Glands that received higher doses showed more Annexin uptake. ΔU in primary tumour and pathological lymph nodes showed large inter-patient differences. A high correlation was observed on an inter-patient level ($r=0.71$, $p=0.006$) between the maximum ΔU in primary tumour and in the lymph nodes.

Conclusions Within the dose range of 0–8 Gy, Annexin-V-scintigraphy showed a radiation-dose-dependent uptake in parotid glands, indicative of early apoptosis during treatment. The inter-individual spread in Annexin uptake in primary tumours could not be related to differences in dose or tumour volume, but the Annexin uptake in tumour and lymph nodes were closely correlated. This effect might represent a tumour-specific apoptotic response.

Keywords Apoptosis · Annexin · Scintigraphy · Head and neck cancer · Parotid gland

Introduction

Apoptosis is an important mechanism of cell death in response to treatment with radiation and many chemotherapeutic agents [1]. To what extent apoptosis contributes to the overall cytotoxic effect of an anti-cancer treatment modality has been the topic of intense research during the last decade [2–4]. The relative contribution of apoptosis to the occurrence of cell death varies greatly both between different tumour types and normal tissues [5].

Recently, *in vivo* imaging of apoptosis has proven to be feasible by using radiolabelled Annexin V [6–10]. This endogenous human protein has a high affinity for membrane-bound lipid phosphatidylserine (PS), which becomes exposed at the outer leaflet of the cell membrane bilayer at an early stage of the apoptotic process [11, 12]. PS then serves as a recognition site for macrophages that digest and remove apoptotic cells. The reproducibility of the ^{99m}Tc -Hynic-Annexin-V scintigraphy has been demonstrated in head and neck squamous cell carcinoma (HNSCC) patients by serial imaging in untreated patients [13] in which the mean difference in uptake was 6%. We have recently demonstrated that ^{99m}Tc -Hynic-rh-Annexin V scintigraphy (TAVS) correlates with radiation-induced cytologically confirmed apoptosis in non-Hodgkin lymphoma [14] and can be used to identify patients that have a favourable prognosis [15].

The current standard of practice for patients with advanced stage HNSCC is treatment with concurrent cisplatin-based chemoradiation [16, 17]. Although this is an effective treatment, it also is accompanied by more severe toxicity than radiation alone. We reasoned that TAVS early during treatment might be used to monitor apoptosis induction in tumour and normal tissue and to give an indication of the radiosensitivity of these structures. In future, this would also offer the possibility to adapt the treatment strategy at an early stage on a patient-by-patient basis.

In the present study, we therefore aimed at assessing the feasibility of TAVS as a non-invasive technique to demonstrate treatment-induced apoptosis *in vivo*, in patients with HNSCC, early during treatment with concurrent chemoradiation. The purpose was to determine the degree of uptake on TAVS in normal tissue, primary tumour and lymph node metastases and to evaluate the treatment-induced Annexin uptake in relation to radiation dose. Furthermore, we questioned whether the differences in uptake would correlate with treatment response.

Materials and methods

Patients included in this study were recruited between January 2004 and March 2005 from a randomised phase III

trial in advanced stage HNSCC, investigating the optimal route of cisplatin delivery during cisplatin-based chemoradiation (RADPLAT). Randomisation was between two treatment arms: Arm 1, standard intravenous (IV) administration of cisplatin 100 mg/m^2 (1 h before radiotherapy at days 1, 22 and 43) or arm 2, high-dose selective intra-arterial (IA) delivery of cisplatin at a dose of 150 mg/m^2 (on days 2, 9, 16 and 23, within 1 h after radiotherapy delivery). Main eligibility criteria included: inoperable squamous cell carcinoma of the oral cavity, oropharynx or hypopharynx, TNM stage T3-4 status of primary oral cavity or oropharyngeal tumours and T2-3-4 for hypopharyngeal tumours, with any N-status, (functionally) inoperable disease, no distant metastases, age at least 18 years, ability to give informed consent and no prior cerebro-vascular accident. Both the randomised trial and the TAVS study were approved by the medical ethics committee of the hospital. Patients were informed about the nature of the study protocol and signed informed consent before enrolment separately for both the randomised trial and the TAVS protocol.

Radiotherapy was given with 4–6 MV photon linear accelerators. Target volume included the primary tumour and the bilateral neck for a dose of 46 Gy in 23 fractions. A boost was given to the known macroscopic tumour extensions at the primary tumour site and lymph node metastases to a dose of 24 Gy in 12 fractions. The total dose delivered was 70 Gy in 35 fractions, five fractions per week, with an overall treatment time of 7 weeks. The radiation technique was either a conventional three-field beam setup (using conventional simulation or virtual simulation with CT scan) or an intensity-modulated radiotherapy (IMRT) plan depending on resources and tumour extent. The IA cisplatin delivery was accomplished by a selective catheterisation procedure using the femoral artery according to the earlier described RADPLAT protocol [18, 19]. Concurrently, with IA cisplatin sodium-thiosulphate was administered to neutralise systemic cisplatin. In both arms, prehydration and posthydration were given.

^{99m}Tc -Hynic-rh-Annexin V scintigraphy, diagnostic imaging, radiation treatment planning and image fusion

Baseline TAVS was performed within 2 weeks before the start of concurrent chemoradiation (average interval 5 days, range 1–8). Post-treatment TAVS was done within 48 h after the start of cisplatin chemotherapy. At the time of post-treatment TAVS, patients had received 6 Gy of radiation in case of IV cisplatin, 8 Gy in case of IA cisplatin. Each patient received an average of 847 MBq (range 714–1032 MBq) of ^{99m}Tc -Hynic-rh-Annexin V (Theseus Imaging Corporation, Boston, USA) by slow intravenous injection 4 h before the planar imaging and single-photon emission tomography (SPECT) imaging. Planar images

were used to assess the biodistribution. SPECT of the head and neck region was acquired by the step-and-shoot mode, one step per 3°, 30 s per frame, matrix size 128×128, using a dual-head gamma camera (Genesis, Philips, Best, The Netherlands) equipped with low-energy, high-resolution collimators. For SPECT reconstructions, an iterative algorithm was used and the images were postfiltered using a Butterworth filter (cutoff frequency 0.35, order 5). The use of absolute quantitative analysis of SPECT data was validated by comparison of iterative and FBP reconstruction methods. Transaxial, coronal and sagittal slices were visually examined to evaluate tracer uptake at the tumour sites and in normal tissues. The intensity of the obtained images was corrected by normalisation for the injected radioactive dose and body weight.

Baseline diagnostic imaging with MRI (1.5-T system; Somatom; Siemens Medical Systems, Erlangen, Germany) or spiral CT (Tomoscan AVE1, Philips, Best, The Netherlands or HiSpeed CT, GE Medical Systems, USA) was performed within 3 weeks before the start of treatment and repeated 6–8 weeks after the end of the treatment for the evaluation of treatment response.

Radiation treatment planning was done with our clinical treatment planning system (TPS; U-MPlan, University of Michigan, Ann Arbor, USA). Six patients were treated by IMRT, and the treatment plans were recalculated for the dose at the time of first post-treatment TAVS. The regions of interest (ROI) were delineated manually for each patient on the CT scan. These included the gross tumor volume (GTV) of the primary tumour and/or lymph nodes, the parotid glands and the submandibular glands. In the other seven patients, a standard three-field technique was used by virtual simulation with a CT scan. In these latter patients, the CT scan was imported into the TPS in which the delineations were done. The treatment fields were reconstructed, and the clinically applied dose distribution at the time of TAVS was recalculated in the TPS. The primary tumour and lymph node volumes were calculated by 3-D reconstruction of the delineated GTV.

SPECT, MRI and CT were performed separately. For the SPECT scan, we obtained reproducibility of the positioning of the head and neck as during RT by the use of immobilisation mask fixed to the table by adhesive tape. All images and the radiation dose data were transferred for image fusion to our in-house developed workstation for co-registration (Worldmatch Workstation) in DICOM format [20]. Keeping the limitations of the mask fixation in mind, it was decided that for more accuracy, matching was performed on different anatomical regions for different ROIs, e.g. for the analysis of parotid glands or oropharyngeal tumours, the co-registration was done in such a way that it ensured adequate matching for that area only. For co-registration of ROIs in the neck (e.g. lymph nodes or

hypopharyngeal tumours), only the neck and vertebral column was used in the matching procedure. Accurate matching of body contours and bone structures was visually verified. SPECT, composite SPECT/SPECT, CT and SPECT/CT images, obtained using a colourwash technique, were simultaneously examined using linked cursor to evaluate Annexin V uptake in tumour and normal tissues.

The tumour and normal tissue uptake at baseline and post-treatment were calculated as follows. ROIs were delineated in the planning CT. Each ROI was projected using the registration transformation onto the baseline and post-treatment SPECT scans. The area was next sampled by 10.000 random points, and for each point, the Annexin uptake was determined in the SPECT scans by trilinear interpolation. Of these 10.000 samples, the maximum and mean values were computed. In this way, the uptake in the ROI was accurately sampled, although the pixel size in the SPECT scans is relatively large (about 5 mm). For the quantification of Annexin uptake, no attenuation correction was performed because the images were obtained on a conventional gamma camera without a hybrid system. Subsequently, the difference (ΔU) between the post-treatment and baseline uptake was determined by subtraction of the baseline scan from the post-treatment scan. The subtraction was performed on a point by point basis for all 10.000 points. Then, the mean or maximum value of the difference of both scans (subtraction scan) was computed and expressed as ΔU . No correction for background activity was made, as this was automatically eliminated by subtraction of the baseline activity from the post-treatment activity, assuming that the background activity is equal in the baseline and post-treatment scan. Radiation dose parameters (mean and maximum dose in cGy) within each ROI were calculated and correlated with corresponding ΔU parameters. It was observed that the maximum ΔU and the mean ΔU were closely related: a linear relationship between both two parameters was found for each ROI (tumour: $r=0.93$, $p<0.0001$; parotid gland: $r=0.94$, $p<0.0001$; submandibular gland: $r=0.90$, $p<0.0001$; lymph node $r=0.94$, $p<0.0001$), indicating that both values would have been representative for the whole ROI.

Evaluation of treatment

Six to eight weeks after the end of treatment, the results of therapy were evaluated by means of radiological investigations (by MRI or CT scan and/or ultrasound) and examination under general anaesthesia, with biopsies taken in case of suspicious findings. For residual disease in the neck at the time of evaluation, salvage neck dissection was performed if the patient was judged operable. Follow-up visits were planned every 3 months in the first year after therapy, every 4 months in the second year and less

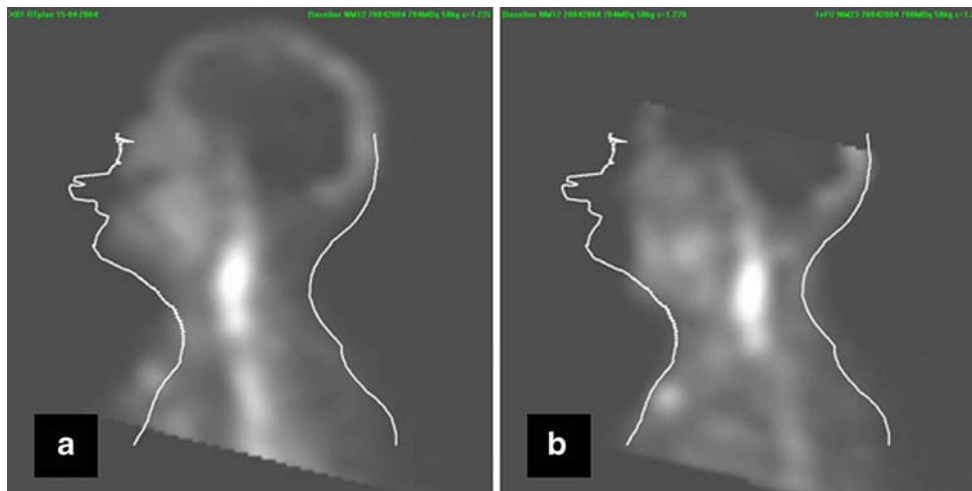


Fig. 1 Sagittal projection of TAVS imaging co-registered with planning CT scan. The *solid line* represents the contour of the patient during RT-planning CT scan, including tongue depressor. The projected image is the TAVS. **a** Baseline TAVS; **b** post-treatment TAVS. Note the mismatch of contours of the head and neck mostly

due to different position of the chin in **b**. The misalignment of the lower neck in **a** is due to the flexion of the neck. For the analysis, the matching procedure was focused on the mandibular region. This patient was excluded from analysis because of misalignment in **b**

frequent thereafter. A follow-up chest X-ray was performed annually.

Statistical analysis

For quantitative comparison of continuous data Student's *t* test was applied. Chi-squared and Fisher's exact test were used for analysis of categorical data. The Pearson and Spearman rank correlation coefficient *r* were used to calculate correlations between Annexin uptake and treatment parameters. Locoregional control and survival data were calculated from the start of treatment using the

Kaplan–Meier method and log rank testing. Two-sided *P* values of <0.05 were considered statistically significant.

Results

Sixteen patients gave their consent for participating in the TAVS study. However, one patient refused post-treatment TAVS scans; in one patient, no CT scan in radiation treatment position was available, and in one patient, co-registration with SPECT was unsuccessful due to misalignment because no immobilisation mask and no tongue

Table 1 Patient, tumour and treatment characteristics

Patient number	Gender	Age (years)	Tumor site	TNM stage	Tumor volume (cm ³)	Max ΔU in primary tumour	Interval cisplatin infusion and Annexin scan (h)	RT technique	Mode of cisplatin administration
1	M	64	Oral cavity	III	21	62	52.2	Conventional 3 field	Intra-arterially
2	M	58	Oropharynx	III	47	203	50.3	IMRT	Intra-arterially
3	F	65	Oropharynx	IV	25	112	53.1	IMRT	Intra-arterially
4	M	55	Oropharynx	III	26	36	53.5	IMRT	Intra-arterially
5	M	49	Hypopharynx	II	13	43	53.3	IMRT	Intra-arterially
6	F	66	Oral cavity	IV	32	135	53.6	Conventional 3 field	Intra-arterially
7	M	60	Oropharynx	IV	147	191	54.3	Conventional 3 field	Intra-arterially
8	M	46	Oropharynx	IV	28	170	52.7	Conventional 3 field	Intra-arterially
9	M	55	Oropharynx	IV	41	42	49.9	IMRT	Intravenously
10	M	57	Oropharynx	IV	25	51	51.7	IMRT	Intravenously
11	M	48	Oropharynx	IV	91	117	51.5	Conventional 3 field	Intravenously
12	M	50	Hypopharynx	IV	100	132	50.3	Conventional 3 field	Intravenously
13	M	26	Oropharynx	IV	105	52	50.1	Conventional 3 field	Intravenously

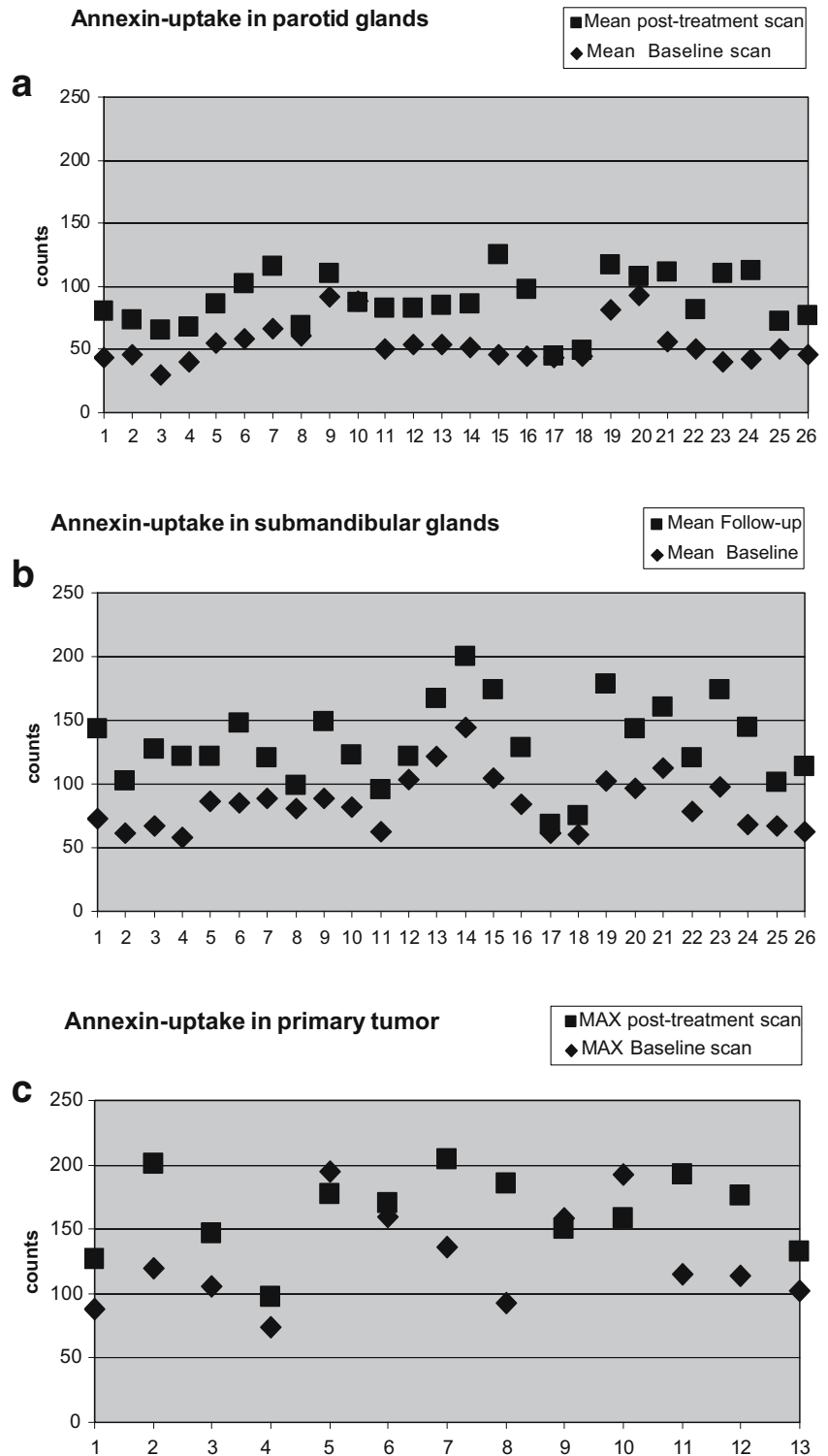
M Male, *F* female, *IMRT* intensity modulated radiotherapy

depressor could be used during SPECT due to pain (Fig. 1). The number of patients included in this analysis on ^{99m}Tc -Hynic-rh-Annexin V scintigraphy in advanced stage HNSCC is therefore 13. The mean age of patients was 53 years (range 26–66 years). See Table 1 for the patient, tumour and treatment characteristics.

Annexin uptake in normal tissue and tumour

At baseline scintigraphy, reproducible physiologic Annexin uptake was detected on the planar images in liver, kidneys, spleen, gall bladder, bone marrow, colon and urinary bladder, as described earlier [7, 14, 21].

Fig. 2 Baseline (*diamonds*) and post-treatment (*squares*) Annexin activity in parotid glands (a), submandibular glands (b) and tumour (c) for all 13 patients. The data for 26 parotid and submandibular glands represent the right and left gland within each patient



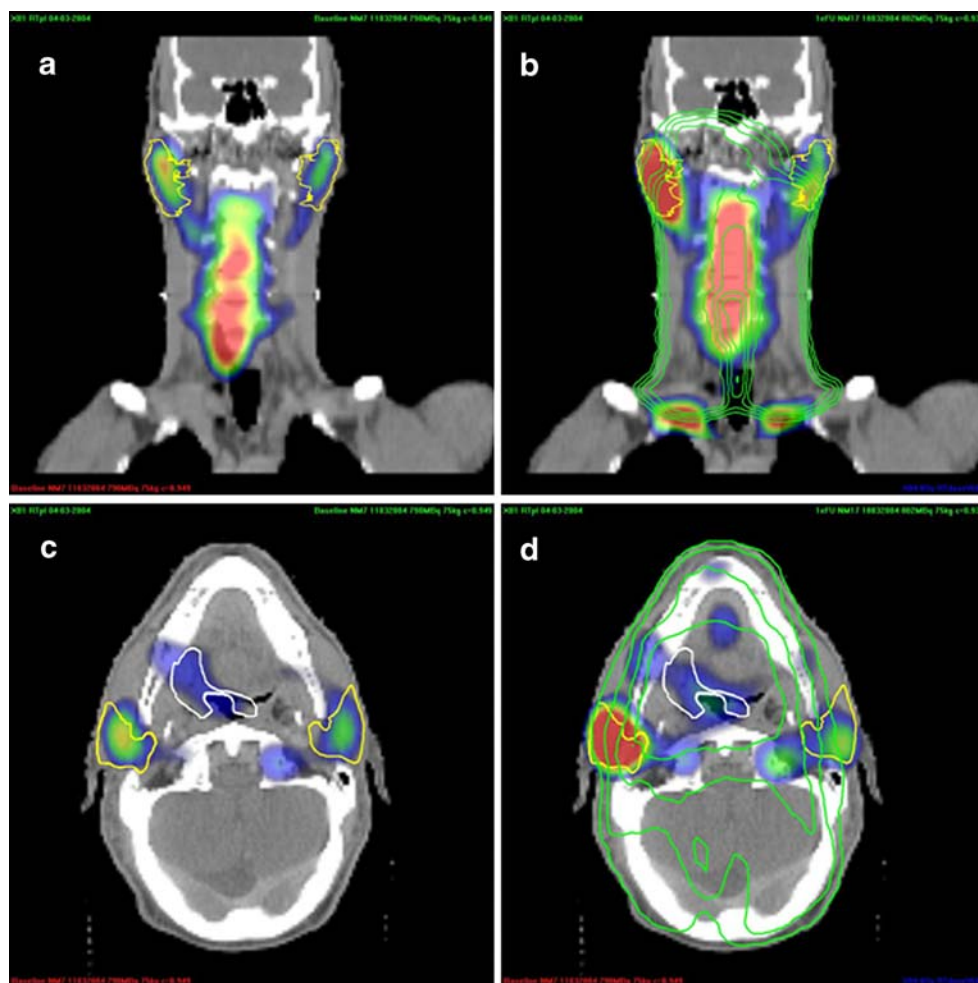
In the parotid glands, weak baseline uptake was present in all cases. The post-treatment TAVS showed moderate to strong increase in uptake in 24 of 26 parotid glands (Fig. 2a). The average of the mean number of counts increased from 55 to 88 ($p < 0.001$). Visual analysis of the increase in uptake showed that these changes were related to the radiation portals and the dose given to the parotid glands (Fig. 3). The difference in Annexin uptake between the post-treatment and baseline TAVS (ΔU) in each parotid gland was correlated with the radiation dose at the time of post-treatment scintigraphy ($n = 13$ patients, $n = 26$ parotids). The mean ΔU showed a positive correlation with the mean radiation dose (Pearson coefficient $r = 0.59$, $p = 0.002$): parotid glands that received a higher dose of radiation showed a higher Annexin uptake (Fig. 4a). The increase in Annexin uptake in parotid glands that were treated with parotid-sparing IMRT was less than in parotid glands that were treated with a conventional three-field technique (IMRT 29 counts, three-field technique 59 counts, $p = 0.02$). The given radiation dose at the time of post-treatment TAVS (6 or 8 Gy) and the mode of cisplatin administration (IA or IV) did not affect the uptake in parotid glands. As

xerostomia scoring was not documented sufficiently detailed in the files, we interviewed patients alive at last follow-up for xerostomia grading for the purpose of this study. In nine patients alive at last follow-up, the treatment-induced Annexin uptake in parotid glands was related to the subjective xerostomia rating using the EORTC QLQ HN-35 questionnaire [22]. No relation could be established in this small set of patients (data not shown).

For the submandibular glands, a similar pattern as with the parotids was observed: absent/weak baseline uptake and moderate to strong increase after the start of chemoradiation (Fig. 2b). The average of the mean number of counts increased from 85 to 132 ($p < 0.001$). No correlation between the ΔU and radiation dose was noted (Fig. 4b), probably as all submandibular glands were located within the high-dose region.

The baseline TAVS showed moderate to strong Annexin uptake in the primary tumour in all patients, indicative of spontaneous apoptosis or necrosis. On the post-treatment TAVS, the uptake in tumour clearly increased in nine cases; in the other four, little or no changes occurred (Fig. 2c). The average of the maximum number of counts increased from

Fig. 3 TAVS imaging co-registered with planning CT scan in frontal plane and axial plane, **a** and **c** at baseline, **b** and **d** after treatment, from patient number 2. The Annexin uptake is represented by colourwash. In **b** and **d**, the isodose lines show the dose distribution in relation to the parotid gland and primary tumour (isodose lines shown, 40, 60, 80 and 95% from outer to inner side of patient). Note the increased treatment-induced Annexin uptake in the right parotid gland, in correspondence to the higher radiation dose distribution, when compared to the left parotid gland. Also note the weak increase in primary tumour Annexin uptake in the right oropharynx after treatment and in the anterior floor of mouth (**d**)



127 to 163 ($p=0.007$). The difference between post-treatment and baseline TAVS (ΔU) in primary tumour was not correlated with primary tumour volume (Pearson coefficient $r=0.39$, $p=0.21$) nor with the mode of chemotherapy administration ($p=0.21$). In nine patients, 17 lymph node metastases were present in the neck (mean lymph node volume 5 cm^3 , range 1–19). The treatment-induced Annexin uptake (maximum ΔU) in primary tumour was positively correlated with the uptake in corresponding lymph node metastases ($r=0.73$, $p=0.004$) as shown in Fig. 5. To verify that the observed effects of Annexin uptake in different structures could not be attributed solely to the administered radioactive dose per patient but was tissue-specific, we

calculated the correlation between the ΔU in tumour and parotid glands. No evidence of such an effect was found ($r=0.28$, $p=0.18$).

Response to treatment, locoregional control and survival

The median follow-up of all patients alive at last follow-up was 30 months (range 24–38). The complete response (CR) rate at the primary tumour site was 85%. CR rate in the neck in the case of nodal metastases was 100%. The overall CR rate was 85%. The estimated locoregional (LR) tumour control rates were 68% at 2 and 3 years. The rates for disease-free survival (DFS) were 54% at 2 and 3 years.

Fig. 4 Correlation plot of mean radiation dose (cGy) and the post-treatment increase in Annexin uptake, mean ΔU , in parotid glands (a), normalised for tracer dose and body weight. Circles represent parotid glands treated with IMRT, triangles parotids treated with conventional technique. In b, the correlation between mean radiation dose (cGy) and the post-treatment increase in Annexin uptake, mean ΔU , in submandibular glands is given

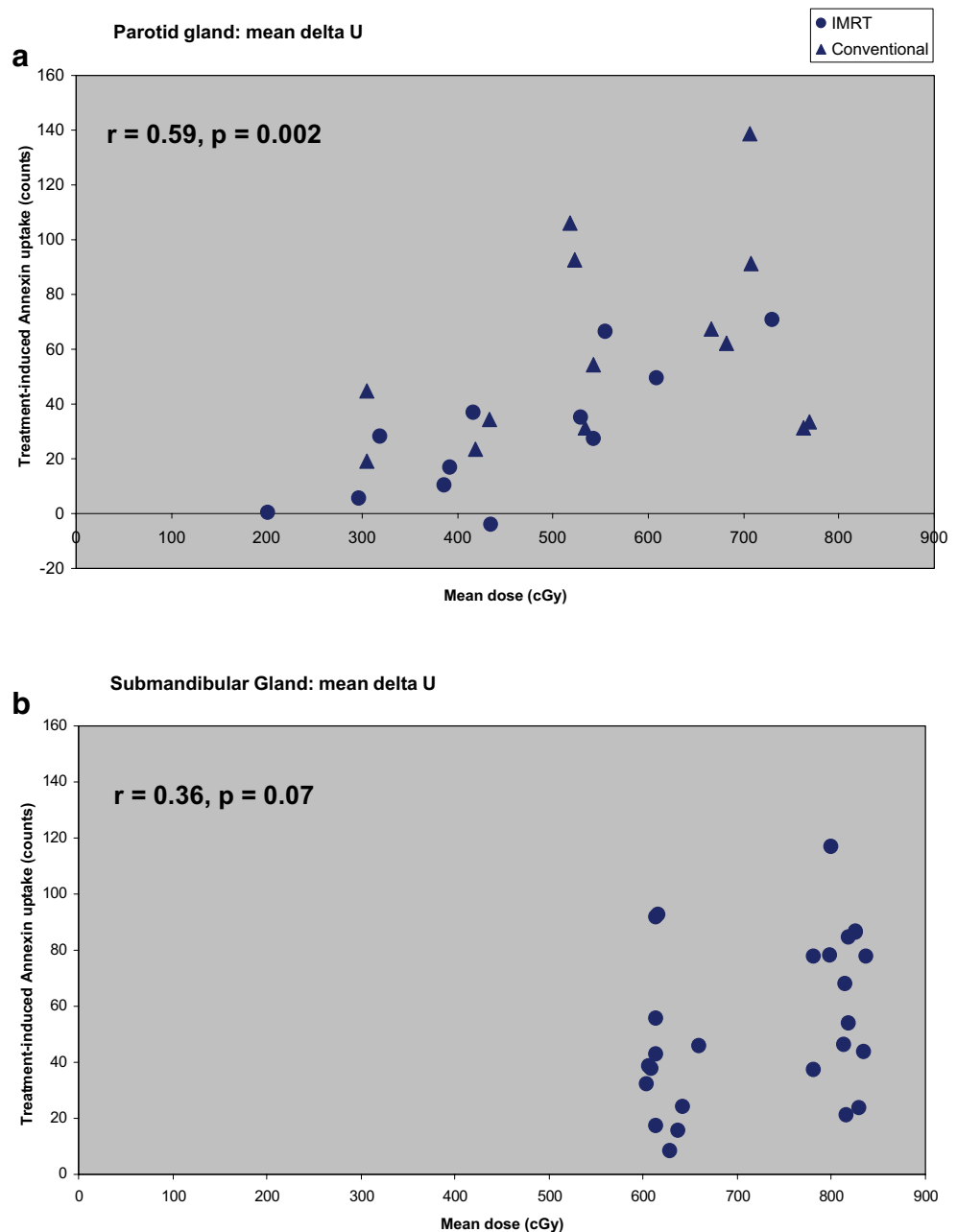
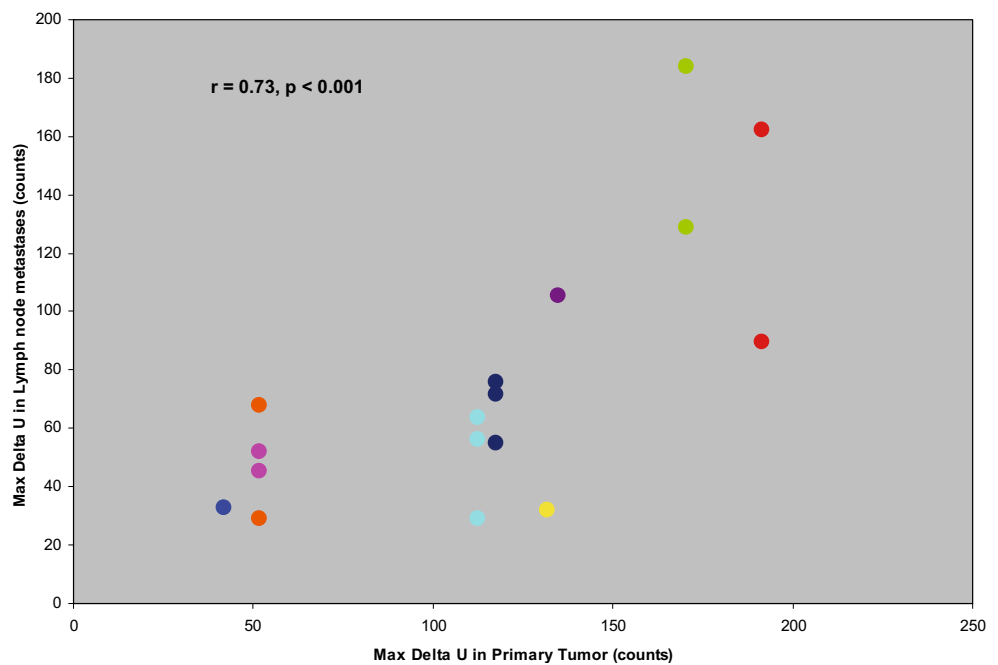


Fig. 5 Correlation plot of the treatment-induced increase in Annexin uptake, maximum ΔU , in primary tumour and lymph node metastases. Each colour represents an individual patient. Some patients had multiple lymph node metastases originating from the same primary tumour. In these cases, multiple values of treatment-induced Annexin uptake in lymph nodes (on the y-axis) correspond to a single value of the primary tumor (on the x-axis)



Overall survival (OS) rates at 2 and 3 years were 62 and 40%, respectively. In this small subset of 13 patients from a larger randomised phase III trial, there were no differences in response rates, LR control, DFS or OS between the two treatment arms (IV vs IA). No correlation could be established between baseline or treatment-induced Annexin uptake (ΔU) and any outcome parameter (response rate, recurrences and/or survival).

Discussion

This study represents our first clinical experience on in vivo imaging of apoptosis with TAVS in HNSCC patients in which we applied co-registration of multiple imaging modalities. By this, we were able to analyse treatment-induced changes in normal and tumour tissue, early during therapy, after one cycle of cisplatin chemotherapy and 6–8 Gy of radiotherapy. Treatment-induced Annexin uptake in the parotid glands could be visualised, indicative of early treatment related apoptosis at mean radiation doses as low as 3–8 Gy (see Fig. 4a) and one course of cisplatin. The Annexin uptake in the parotids showed a radiation dose-response relationship: Glands that had received higher doses of radiation demonstrated increased Annexin uptake.

Loss of parotid gland function, leading to xerostomia, is an important long-term side effect of radiotherapy, affecting quality of life of patients. It has well been shown by scintigraphy studies [23] and by salivary flow rate studies [24] that reduction of radiation dose to the parotid glands can maintain parotid function, decrease xerostomia and improve quality of life. Most studies on salivary gland

function are performed after a full course of RT (typically 60–70 Gy in 6–7 weeks) [23–26]. Our study design with early in vivo imaging indicated that already after low dose of RT (6–8 Gy), parotid glands may be affected and that the physiologic process leading to loss of parotid gland function already starts early. This is in agreement with observations in experimental rodent studies in which apoptosis was induced early, after doses of up to 5 Gy [27]. Similar results were obtained in a monkey model, with early radiation induced apoptosis of serous acinar cells of salivary glands [28]. It was suggested that these early effects are mainly responsible for the acute sialoadenitis, which, at higher RT doses, might progress in chronic xerostomia by damage to and depletion of ductal stem cells within the gland. In the nine patients assessed for xerostomia, no relation could be established with subjective salivary gland function after radiotherapy and parotid gland Annexin uptake. However, the significance of this analysis is limited, as we assessed both parotid glands separately by TAVS, and xerostomia questionnaires give an overall impression of function. We did not include follow-up salivary flow studies. In short, our results indicate indirect evidence of early radiation-induced salivary gland damage and, in future studies, this needs to be correlated with functional outcome parameters.

Due to the large inter-patient variability in the baseline TAVS (Fig. 2c), the subtraction method for assessing treatment-induced changes was chosen over a relative method (e.g. percentage change). In this figure, it is important to notice that the maximum uptake value of the baseline and post-treatment scan might be located in different points within the tumour ROI. Therefore, these

data cannot be simply subtracted, but for the calculation of the maximum ΔU in primary tumour and lymph nodes, the baseline scan was first subtracted from the post-treatment scan, and, subsequently, these parameters were calculated from the subtraction scan. The treatment-induced Annexin uptake in primary tumour and pathological lymph nodes showed a positive correlation: Patients with primary tumours with a high Annexin uptake also appeared to have lymph node metastases with high Annexin uptakes. The ΔU in primary tumour and lymph node metastases showed large inter-patient differences (Fig. 5). This variation could not be attributed to differences in the route of cisplatin administration (intravenous or intra-arterial chemoradiation), nor to the radiation doses given (6 or 8 Gy), nor to the primary tumour volume. This positive correlation for ΔU in primary tumour and lymph nodes as well as the large inter-patient differences might represent a tumour-specific apoptotic response.

In our series, repositioning of the patient during SPECT scan in RT position was standard procedure, but due to the limitations in fixation, not optimal. The repositioning facilitated the co-registration of SPECT and CT scan. In one patient, misalignment occurred because the positioning was not accurate due to the fact that the RT position could not be reproduced (Fig. 1). So, for co-registration of (functional) imaging to RT-planning CT scan data in HNSCC, we recommend improvements from our protocol to obtain a reproducible positioning, like the use of an immobilisation mask fixed to the SPECT table, the use of the same mattress under the patient and a laser alignment system. In ongoing studies, we have now incorporated these. In the current series, no attenuation correction was applied because the images were obtained on a conventional gamma camera without a hybrid system. For the purpose of this study, the quantification of Annexin uptake remains valid, as we used the relative increase from baseline to post-treatment uptake, and the degree of attenuation will be equal on both scans.

In this small series of HNSCC, the treatment-induced Annexin uptake (ΔU) in primary tumour did not predict outcome: No correlation between Annexin uptake and early response was observed probably partly due to the high initial response rates (85%). In addition, TAVS also did not predict the locoregional control rates within the first 2 years of follow-up. In our previous experience on TAVS in other tumour sites (mainly lymphoma), a strong correlation has been found between early response (within 3 months) and Annexin uptake [15]. One explanation for the lack of correlation might be that in the current series, these advanced stages HNSCC with large tumours harbour more necrosis, which is also detected by TAVS because of accessibility of PS at the necrotic cell membrane [29]. Van de Wiele et al. [8] showed that in HNSCC, Annexin

scintigraphy correlated with histopathological apoptosis (using TUNEL assay) only in the absence of necrosis. Indeed, in this series, baseline Annexin uptake in the HNSCC patients was clearly demonstrated, whereas it was not present in our previous study in lymphoma patients [15]. This may suggest the presence of necrosis in large tumours from solid origin. Other factors that may affect Annexin uptake are the intra- and peri-tumoural lymphocyte infiltration [30]. For the future, we plan to increase the number of HNSCC patients to undergo the TAVS imaging to prove whether or not it can be used for outcome prediction as it was shown in patients with malignant lymphoma and non-small cell lung cancer [14, 15].

In conclusion, co-registration of Annexin V scintigraphy with radiotherapy-planning CT scan showed a radiation-dose-dependent uptake in parotid glands, indicative of early apoptosis during treatment. The inter-individual spread in Annexin uptake in primary tumours could not be related to differences in treatment schedule or tumour volume, but the Annexin uptake in tumour and lymph nodes were closely correlated. This effect might represent a tumour-specific apoptotic response.

Conflicts of interest None declared.

References

1. Dive C, Evans CA, Whetton AD. Induction of apoptosis-new targets for cancer chemotherapy. *Semin Cancer Biol* 1992;3:417–27.
2. Hickman JA. Apoptosis induced by anticancer drugs. *Cancer Metastasis Rev* 1992;11:121–39.
3. Verheij M, Bartelink H. Radiation-induced apoptosis. *Cell Tissue Res* 2000;301:133–42.
4. Tamm I, Schriever F, Dorken B. Apoptosis: implications of basic research for clinical oncology. *Lancet Oncol* 2001;2:33–42.
5. Meyn RE, Stephens LC, Milas L. Programmed cell death and radioresistance. *Cancer Metastasis Rev* 1996;15:119–31.
6. Blankenberg FG, Katsikis PD, Tait JF, Davis RE, Naumovski L, Ohtsuki K, et al. In vivo detection and imaging of phosphatidylserine expression during programmed cell death. *Proc Natl Acad Sci USA* 1998;95:6349–54.
7. Kemerink GJ, Liu X, Kieffer D, Ceysens S, Mortelmans L, Verbruggen AM, et al. Safety, biodistribution, and dosimetry of ^{99m}Tc -HYNIC-annexin V, a novel human recombinant annexin V for human application. *J Nucl Med* 2003;44:947–52.
8. Van De Wiele C, Lahorte C, Vermeersch H, Loose D, Mervillie K, Steinmetz ND, et al. Quantitative tumor apoptosis imaging using technetium- ^{99m}Tc -HYNIC annexin V single photon emission computed tomography. *J Clin Oncol* 2003;21:3483–7.
9. Kuge Y, Sato M, Zhao S, Takei T, Nakada K, Seki KI, et al. Feasibility of ^{99m}Tc -annexin V for repetitive detection of apoptotic tumor response to chemotherapy: an experimental study using a rat tumor model. *J Nucl Med* 2004;45:309–12.
10. Ogura Y, Krams SM, Martinez OM, Kapiwoda S, Higgins JP, Esquivel CO, et al. Radiolabeled annexin V imaging: diagnosis of allograft rejection in an experimental rodent model of liver transplantation. *Radiology* 2000;214:795–800.

11. Fadok VA, Voelker DR, Campbell PA, Cohen JJ, Bratton DL, Henson PM. Exposure of phosphatidylserine on the surface of apoptotic lymphocytes triggers specific recognition and removal by macrophages. *J Immunol* 1992;148:2207–16.
12. van Engeland M, Kuijpers HJ, Ramaekers FC, Reutelingsperger CP, Schutte B. Plasma membrane alterations and cytoskeletal changes in apoptosis. *Exp Cell Res* 1997;235:421–30.
13. Vermeersch H, Ham H, Rottey S, Lahorte C, Corsetti F, Dierckx R, et al. Intraobserver, interobserver, and day-to-day reproducibility of quantitative ^{99m}Tc -HYNIC annexin-V imaging in head and neck carcinoma. *Cancer Biother Radiopharm* 2004;19:205–10.
14. Haas RL, de Jong D, Valdes Olmos RA, Hoefnagel CA, Van Den Heuvel I, Zerp SF, et al. In vivo imaging of radiation-induced apoptosis in follicular lymphoma patients. *Int J Radiat Oncol Biol Phys* 2004;59:782–7.
15. Kartachova M, Haas RL, Valdes Olmos RA, Hoebbers FJ, van Zandwijk N, Verheij M. In vivo imaging of apoptosis by (^{99m}Tc -Annexin V scintigraphy: visual analysis in relation to treatment response. *Radiother Oncol* 2004;72:333–9.
16. Pignon JP, Bourhis J, Domenge C, Designe L. Chemotherapy added to locoregional treatment for head and neck squamous-cell carcinoma: three meta-analyses of updated individual data. MACH-NC Collaborative Group. Meta-analysis of chemotherapy on head and neck cancer. *Lancet* 2000;355:949–55.
17. Bourhis J. and C.Amand, J.-P. Pignon on behalf of the MACH-NC Collaborative Group. Update of MACH-NC (meta-analysis of chemotherapy in head & neck cancer) database focused on concomitant chemoradiotherapy. *Journal of Clinical Oncology* 22 No 14S (July 15 Supplement). ASCO Annual Meeting Proceedings (Post-Meeting Edition) 2004; p. 5505.
18. Balm AJ, Rasch CR, Schornagel JH, Hilgers FJ, Keus RB, Schultze-Kool L, et al. High-dose superselective intra-arterial cisplatin and concomitant radiation (RADPLAT) for advanced head and neck cancer. *Head Neck* 2004;26:485–93.
19. Robbins KT, Kumar P, Regine WF, Wong FS, Weir AB, III, Flick P, et al. Efficacy of targeted supradose cisplatin and concomitant radiation therapy for advanced head and neck cancer: the Memphis experience. *Int J Radiat Oncol Biol Phys* 1997;38:263–71.
20. Wolthaus JW, van Herk M, Muller SH, Belderbos JS, Lebesque JV, de Bois JA, et al. Fusion of respiration-correlated PET and CT scans: correlated lung tumour motion in anatomical and functional scans. *Phys Med Biol* 2005;50:1569–83.
21. Belhocine T, Steinmetz N, Hustinx R, Bartsch P, Jerusalem G, Seidel L, et al. Increased uptake of the apoptosis-imaging agent (^{99m}Tc) recombinant human Annexin V in human tumors after one course of chemotherapy as a predictor of tumor response and patient prognosis. *Clin Cancer Res* 2002;8:2766–74.
22. Meirovitz A, Murdoch-Kinch CA, Schipper M, Pan C, Eisbruch A. Grading xerostomia by physicians or by patients after intensity-modulated radiotherapy of head-and-neck cancer. *Int J Radiat Oncol Biol Phys* 2006;66:445–53.
23. Munter MW, Karger CP, Hoffner SG, Hof H, Thilmann C, Rudat V, et al. Evaluation of salivary gland function after treatment of head-and-neck tumors with intensity-modulated radiotherapy by quantitative pertechnetate scintigraphy. *Int J Radiat Oncol Biol Phys* 2004;58:175–84.
24. Eisbruch A, Ten Haken RK, Kim HM, Marsh LH, Ship JA. Dose, volume, and function relationships in parotid salivary glands following conformal and intensity-modulated irradiation of head and neck cancer. *Int J Radiat Oncol Biol Phys* 1999;45:577–87.
25. Valdes Olmos RA, Keus RB, Takes RP, van Tinteren H, Baris G, Hilgers FJ, et al. Scintigraphic assessment of salivary function and excretion response in radiation-induced injury of the major salivary glands. *Cancer* 1994;73:2886–93.
26. Buus S, Grau C, Munk OL, Rodell A, Jensen K, Mouridsen K, et al. Individual radiation response of parotid glands investigated by dynamic (^{11}C -methionine PET. *Radiother Oncol* 2006;78:262–9.
27. Paardekooper GM, Cammelli S, Zeilstra LJ, Coppes RP, Konings AW. Radiation-induced apoptosis in relation to acute impairment of rat salivary gland function. *Int J Radiat Biol* 1998;73:641–8.
28. Stephens LC, Schultheiss TE, Price RE, Ang KK, Peters LJ. Radiation apoptosis of serous acinar cells of salivary and lacrimal glands. *Cancer* 1991;67:1539–43.
29. Brouckaert G, Kalai M, Krysko D, Saelens X, Vercaemmen D, Ndlovu M, et al. Phagocytosis of necrotic cells by macrophages is phosphatidylserine dependent and does not induce inflammatory cytokine production. *Mol Biol Cell* 2004;15:1089–100.
30. Badoual C, Hans S, Rodriguez J, Peyrard S, Klein C, Agueznyan Nel H, et al. Prognostic value of tumor-infiltrating CD4⁺ T-cell subpopulations in head and neck cancers. *Clin Cancer Res* 2006;12:465–72.